The Astrophysical Journal Letters, 996:L39 (10pp), 2026 January 10 https://doi.org/10.3847/2041-8213/ae2656

Compelling Evidence for a Harmonic in the Light Curve of the Supermassive Black Hole Binary Candidate PKS J1309+1154

A. C. S. Readhead[1,2], M. F. Aller[3], A. G. Sullivan[4], R. D. Blandford[4], P. Mróz[5], P. V. De la Parra[6], B. Molina[6], E. R. Most[7,8], M. L. Lister[9], A. Synani[2,10], H. Aller[3], M. C. Begelman[11], Y. Ding[12], M. J. Graham[13], F. Harrison[12], T. Hovatta[14,15,16], I. Liodakis[2], W. Max-Moerbeck[17], V. Pavlidou[2,10], T. J. Pearson[1], V. Ravi[1], R. A. Reeves[6], T. Surti[1], K. Tassis[2,10], S. E. Tremblay[18], and J. A. Zensus[19]
[1] Owens Valley Radio Observatory, California Institute of Technology, Pasadena, CA 91125, USA; acr@caltech.edu
[2] Institute of Astrophysics, Foundation for Research and Technology-Hellas, GR-70013 Heraklion, Greece
[3] Department of Astronomy, University of Michigan, 323 West Hall, 1085 S. University Avenue, Ann Arbor, MI 48109, USA
[4] Kavli Institute for Particle Astrophysics and Cosmology, Department of Physics, Stanford University, Stanford, CA 94305, USA
[5] Astronomical Observatory, University of Warsaw, Al. Ujazdowskie 4, 00-478 Warszawa, Poland
[6] CePIA, Astronomy Department, Universidad de Concepción, Casilla 160-C, Concepción, 4070386, Chile
[7] TAPIR, Mailcode 350-17, California Institute of Technology, Pasadena, CA 91125, USA
[8] Walter Burke Institute for Theoretical Physics, California Institute of Technology, Pasadena, CA 91125, USA
[9] Department of Physics and Astronomy, Purdue University, 525 Northwestern Avenue, West Lafayette, IN 47907, USA
[10] Department of Physics and Institute of Theoretical and Computational Physics, University of Crete, GR-70013 Heraklion, Greece
[11] JILA, University of Colorado and National Institute of Standards and Technology, 440 UCB, Boulder, CO 80309-0440, USA
[12] Cahill Center for Astronomy and Astrophysics, California Institute of Technology, Pasadena, CA 91125, USA
[13] Division of Physics, Mathematics, and Astronomy, California Institute of Technology, Pasadena, CA 91125, USA
[14] Finnish Centre for Astronomy with ESO (FINCA), University of Turku, FI-20014 University of Turku, Finland
[15] Aalto University Department of Electronics and Nanoengineering, PL 15500, FI-00076 Espoo, Finland
[16] Aalto University Metsähovi Radio Observatory, Metsähovintie 114, 02540, Kylmälä, Finland
[17] Departamento de Astronomía, Universidad de Chile, Camino El Observatorio 1515, Las Condes, Santiago, 7591245, Chile
[18] National Radio Astronomy Observatory, 1011 Lopez Road, Socorro, NM 87801, USA
[19] Max-Planck-Institut für Radioastronomie, Auf dem Hügel 69, D-53121 Bonn, Germany
Received 2025 November 12; revised 2025 November 28; accepted 2025 November 28; published 2026 January 8

Abstract

We recently discovered a supermassive black hole binary (SMBHB) candidate, PKS J1309+1154, in the combined 46 yr University of Michigan Radio Astronomy Observatory (UMRAO) plus Owens Valley Radio Observatory (OVRO) blazar monitoring programs at 14.5/15 GHz. The light curve of PKS 1309+1154 exhibits a 17.9 yr periodicity. We also reported a hint of a first harmonic with a 9 yr periodicity in this object. Further analysis of the PKS J1309+1154 light curve provides compelling evidence that both the fundamental and the harmonic are real, confirming the existence of real periodicities in blazar light curves. This is the first case, to our knowledge, of watertight evidence for a fundamental periodicity and a harmonic periodicity in a blazar light curve. It makes PKS J1309+1154 a *strong* SMBHB candidate and thus the third such candidate to be revealed through long-term radio monitoring, the other two being PKS J0805–0111 and PKS 2131–021, both discovered through the OVRO 40 m Telescope monitoring program. It is argued that hundreds of SMBHB candidates will be discovered by the combination of the South Pole Telescope, the Vera Rubin Observatory, and the Simons Observatory. Coherent searches for gravitational waves from a network of SMBHB candidates, starting immediately, are strongly motivated.

Unified Astronomy Thesaurus concepts: Supermassive black holes (1663); Blazars (164); Relativistic jets (1390)

1. Introduction

The recently discovered evidence for a stochastic background of gravitational waves with periods of months to years (G. Agazie et al. 2023a, 2023b, 2023c; EPTA Collaboration et al. 2023; A. Zic et al. 2023; N. Agarwal et al. 2025; M. T. Miles et al. 2025) relies on millisecond pulsar arrays for the timing[20] and is thought to be due to supermassive black hole binaries (SMBHBs; G. Agazie et al. 2023b; N. Agarwal et al. 2025). This has spurred searches for periodicities in blazar light curves, which have the potential of revealing important clues to the dynamics of the central engines, powered by SMBHs, in active galactic nuclei (AGNs; M. C. Begelman et al. 1984). The phenomenology of AGNs, as revealed through their light curves, has been a challenging area of study, because the expected timescales of any periodicities arising from the dynamics of their central engines range from months to decades. This is due to the fact that the masses of the SMBHs in blazars are typically $10^7 M_\odot$–$10^{10} M_\odot$ (R. Blandford et al. 2019), and very close binaries are unlikely to be seen because, due to gravitational radiation, they spend little time at small separations (M. C. Begelman et al. 1980).

Until recently, the most compelling case has been that of OJ 287 (e.g., H. J. Lehto & M. J. Valtonen 1996; M. J. Valtonen 2007; M. J. Valtonen et al. 2008, 2016, 2023; P. Pihajoki et al. 2013; S. Britzen et al. 2018; S. Komosa et al. 2023). OJ 287 is,

[20] There were two crucial steps in the discovery of millisecond pulsars: (i) the discovery of interplanetary scintillation, at Galactic latitude $-0.^\circ3$, in 4C 21.53 by A. C. S. Readhead & A. Hewish (1974), which first drew attention to the singular nature of this object—see A. C. S. Readhead (2024); and (ii) the discovery of millisecond pulses from 4C 21.53W by D. C. Backer et al. (1982).

in many respects, a typical blazar. At radio, optical, and gamma-ray energies, it exhibits bright flares, of duration ranging from weeks to several months, which dominate its light curve (H. J. Lehto & M. J. Valtonen 1996; P. A. Hughes et al. 1998; A. Ciaramella et al. 2004; J. A. Hodgson et al. 2017).

Our understanding of the phenomenology of blazar light curves is now changing, owing to the large (∼1830 blazars), high-cadence (3–7 days), long-term (2008–present), 15 GHz monitoring campaign of the 40 m Telescope of the Owens Valley Radio Observatory (OVRO; J. L. Richards et al. 2011) and the mid-1970s–30 June 2012 monitoring campaign of the University of Michigan Radio Astronomy Observatory (UMRAO; H. D. Aller et al. 1985; M. F. Aller et al. 2014), which has 83 frequently observed blazars in common with the OVRO sample. The blazars in common in these two samples have therefore been monitored at high cadence for 46 yr. These two datasets are unparalleled in numbers, cadence, and duration for studying long-term variations in blazars.

These monitoring campaigns have revealed that not all blazar light curves are dominated by short-lived flares of duration from weeks to months. Some are dominated by strong slowly varying features, of duration from months to years, upon which shorter-lived smaller-amplitude flux density variations are imprinted.

In the case of PKS 2131–021, S. O'Neill et al. (2022; hereafter, Paper I) and S. Kiehlmann et al. (2025; hereafter, Paper II) have shown that coherent 4.75 yr sinusoidal variations, which cannot be ascribed to the steep spectrum (the "red noise tail") of the power spectral density (PSD) of the variations, are observed from 2.7 GHz to optical frequencies.

In PKS J0805–0111, P. V. de la Parra et al. (2025) and A. D. Hincks et al. (2025) have shown that strong coherent sinusoidal variations are present from 15 GHz to 225 GHz. In addition, the combined UMRAO+OVRO monitoring campaign has recently discovered a third blazar, PKS J1309+1154 (B. Molina et al. 2025; hereafter, Paper III), with a light curve dominated by coherent sinusoidal variations with a period of 17.9 yr from 15 GHz to 104 GHz. Furthermore, in addition to the strong sinusoidal emission, evidence of a possible harmonic was found in the radio light curve of PKS J1309+1154.

The dominant variations in these three blazars are remarkably sinusoidal and have been explained by the "kinetic orbital" model, in which the periodicity is ascribed to orbital motion in an SMBHB (E. Sobacchi et al. 2017; Paper I). Further, more self-consistent modeling of the interior jet emission has successfully explained the multiwavelength phenomenology of PKS 2131–021 and PKS J0805–0111 (A. G. Sullivan et al. 2025; hereafter, Paper IV).

In this paper, we carry out an intensive study of the 46 yr 14.5/15 GHz light curve of PKS J1309+1154. We provide compelling evidence to reject the null hypothesis that the light curve of PKS J1309+1554 does not contain the harmonic found in Paper III. We believe that this is the first time that compelling evidence for a harmonic has been found in the light curve of a blazar. This is vitally important, because the existence of a harmonic constitutes proof of the reality of the fundamental. It is important to note that the evidence for this harmonic is *not* based on the generalized Lomb–Scargle (GLS) spectrum analysis (N. R. Lomb 1976; J. D. Scargle 1982; M. Zechmeister & M. Kürster 2009), which was shown using simulations in Paper III to produce an average of four nonexistent harmonics per simulation. This is not due to the GLS method but to the steep slope of the PSD and random flares in blazars, which therefore require particular caution in *any* spectral analysis.

We conclude that, in view of the harmonic we have detected, PKS J1309+1154 is a *strong* SMBHB candidate. The discovery of a harmonic in a blazar light curve greatly increases the predictive power of searches for SMBHB candidates in blazar light curves.

For consistency with our other papers, we assume the following cosmological parameters: $H_0 = 71\ \mathrm{km\ s^{-1}\ Mpc^{-1}}$, $\Omega_m = 0.27$, and $\Omega_\Lambda = 0.73$ (E. Komatsu et al. 2009). None of the conclusions would be changed were we to adopt the best model of the Planck Collaboration (Planck Collaboration et al. 2020).

2. The Observations

UMRAO carried out a blazar monitoring program on the 26 m Telescope from the mid-1970s to 30 June, 2012 (H. D. Aller et al. 1985; M. F. Aller et al. 2014). Dual linearly polarized feed horns symmetrically straddling the prime focus fed a broadband receiver with bandwidth of 1.68 GHz centered on 14.5 GHz. An on–on observing technique alternated the beams on the source in order to compensate for the ground spillover and atmospheric effects.

The OVRO 40 m Telescope monitoring program was started in 2008 and has run continuously since that time. The telescope has a dual-symmetric-beam system. Before 2014 the system had a Dicke-switched receiver with a 3 GHz bandwidth centered on 15 GHz. In 2014, the Dicke-switched receiver was replaced by a correlation receiver with bandwidth of 4.2 GHz centered on 15.5 GHz. Throughout this Letter, we use 15 GHz for the generic OVRO frequency. The dual switching system, which greatly reduces atmospheric and ground spillover effects, has been described by A. C. S. Readhead et al. (1989), and details of the 40 m monitoring program are given in J. L. Richards et al. (2011).

3. The Fundamental and First Harmonic Periodicities in PKS J1309+1154

The combined UMRAO+OVRO 14.5/15 GHz light curve of PKS J1309+1154 is shown in Figure 1(a). The UMRAO and OVRO wideband receivers provide considerable overlap in frequency. The least-squares fit to the light curve of a sine wave + trend (black curve) has a (fundamental) period of 6551 days and a trend of $-0.00755\ \mathrm{Jy\ yr^{-1}}$. When a harmonic is included in the fit, the values are slightly different (a fundamental period of 6550 days and a trend of $-0.00769\ \mathrm{Jy\ yr^{-1}}$). The fitting was done using the maximum likelihood method described in detail in Papers I and II and summarized in Appendix A. An interesting feature of the fit without the harmonic is that the data clearly oscillate about the fundamental + trend fit shown by the black curve four times per cycle. The residual light curve after subtracting the fundamental + trend is shown in Figure 1(b). The least-squares sine-wave fit to the residual light curve is shown by the green solid curve in Figure 1(b). In Figure 1(a), the heavy dashed green curve shows the sum of the fundamental sine wave + trend + harmonic. In Paper III, it was suggested only that there was a hint of a harmonic, and it was pointed out that

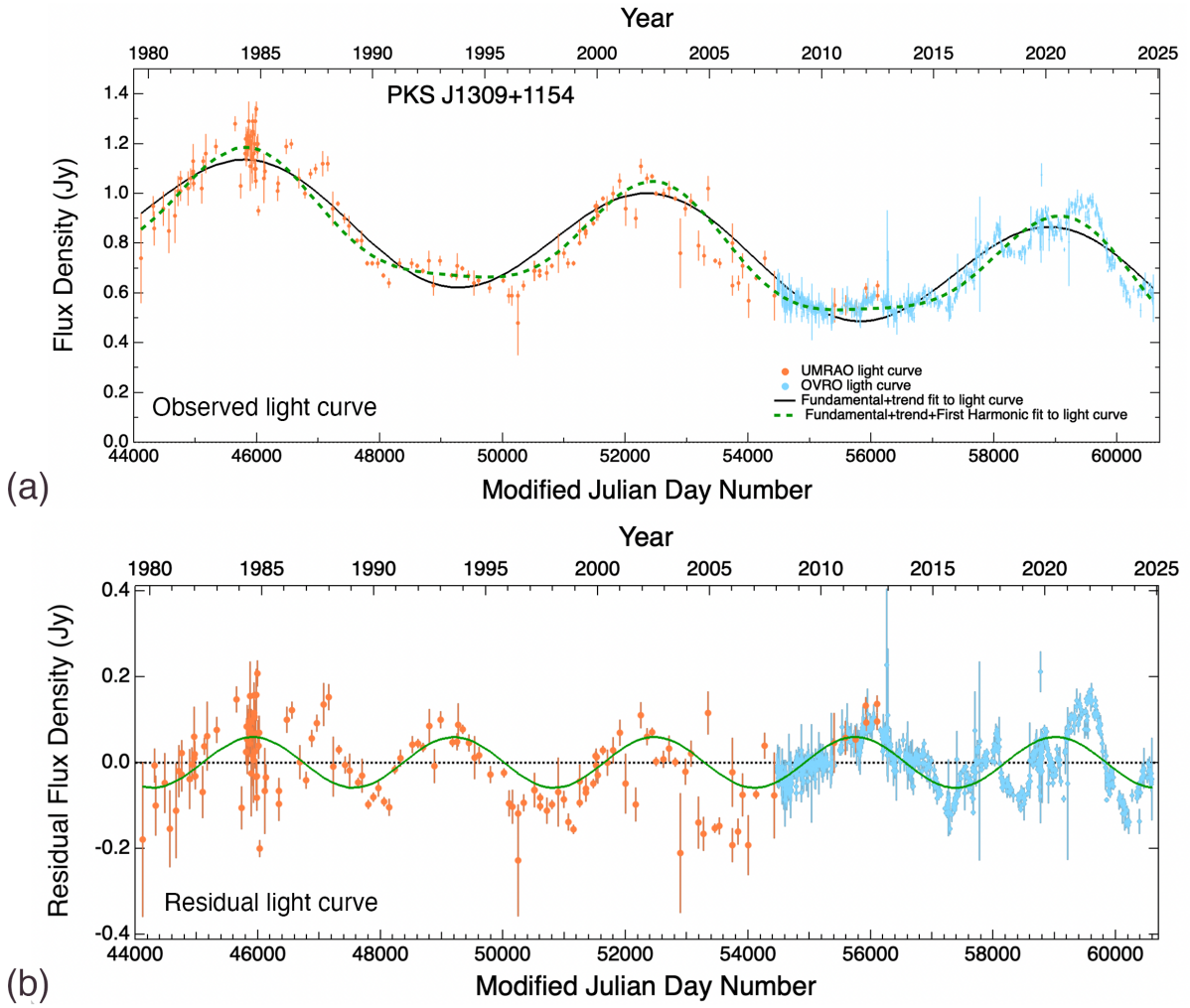

Figure 1. The PKS J1309+1154 fundamental and harmonic periodicities. The orange and blue symbols denote the UMRAO and OVRO data, respectively. (a) The observed light curve. (b) The residual light curve after the subtraction of the black curve in (a), which is the least-squares sine-wave + trend fit to the observed light curve. The solid green curve in (b) shows the fit of the least-squares sine wave to the residual light curve, which has a period of the first harmonic of the fundamental (see the text). The green dashed line in (a) shows the combined fundamental + trend + harmonic.

the frequency of the harmonic is twice that of the fundamental, and also that the harmonic is in phase with the fundamental.

In Paper III, we carried out our standard (see Paper I) significance test based on simulations and showed that the fundamental is significant at the 2.3σ level. This is the *global* significance—i.e., the significance given that we had no *a priori* knowledge of the period (see Paper I). In Paper III, we tentatively interpreted the data to indicate that the light curve of PKS J1309+1154 has a harmonic of twice the frequency in phase with the fundamental. We have now carried out the same statistical analysis on the residual of the PKS J1309+1154 light curve after subtracting the fundamental + trend, shown in Figure 1(b). The local significance of the harmonic, based on the fact that we are looking for a signal of known frequency, is 2.3σ, and the alternate peaks of the harmonic align to within 5% of a cycle of the harmonic. These numbers strongly suggest that the harmonic is real, but they are not compelling.

We now examine the light curve of PKS J1309+1154 in detail. In Table 1, we show the terms we use for the different datasets we consider and their corresponding MJD ranges and dates. We assume a fundamental period of 6550 days. Over the 46 yr duration of the light curve, the fundamental went through 2.57 "cycles." In principle, we could start our first cycle at the beginning of the observations in 1979, but it simplifies the analysis to start the first cycle at the first zero of the harmonic at MJD 45256 (1982 October 14). We therefore label the partial cycle at the beginning "Cycle 0." In each cycle, there are four "sections," equal to half the period of the harmonic, of length 1637.5 days. This gives us 11 separate "regions" where the harmonic lies alternately on one side of the fundamental or the other.

In Figure 2, we show the light curve of PKS J1309+1154 with the 11 regions demarcated by the zero crossings of the harmonic indicated by the vertical black dashed lines. Three very interesting features of this fit of the fundamental + harmonic are:

1. The harmonic creates a flat portion, lasting about 8 yr, i.e., 45% of the fundamental cycle, straddling the minima in the fundamental. This flat portion was observed from 1990 to 1998 and again from 2008 to 2016. It is thus predicted to appear again from 2026 to 2034.

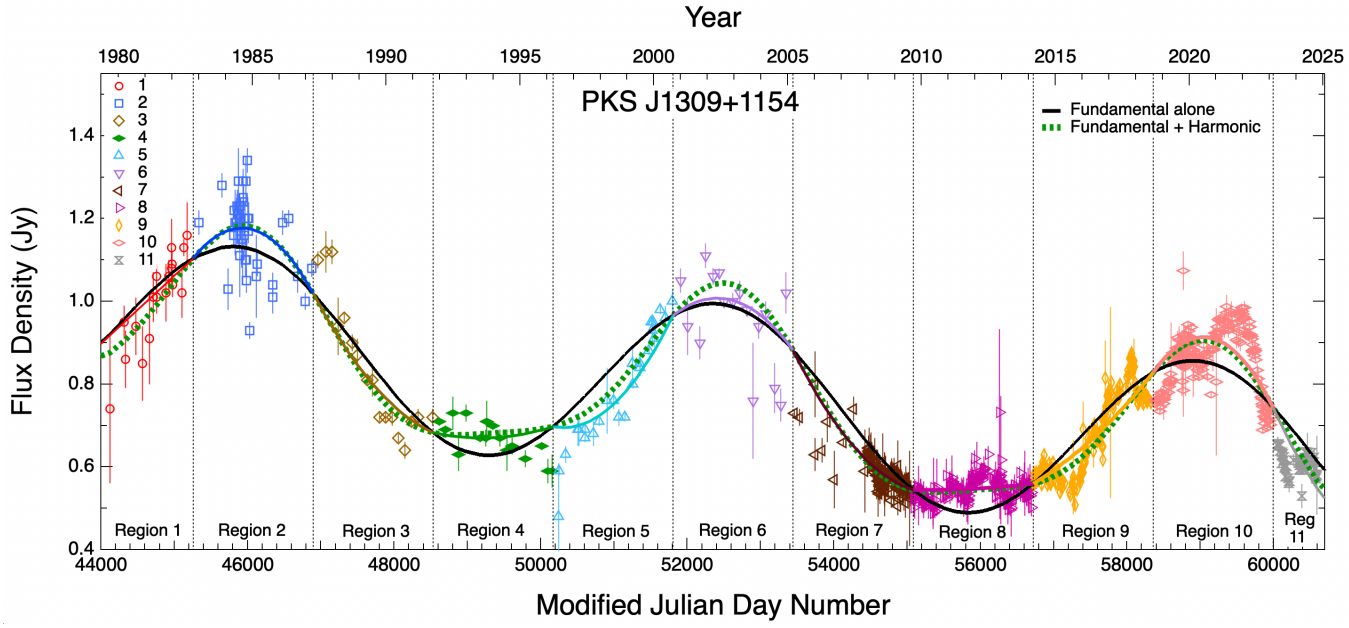

Figure 2. The PKS J1309+1154 light curve analyzed in the 11 distinct regions where the harmonic crosses zero, demarcated by the vertical dashed lines. In each region, a quadratic polynomial has been fitted to the light curve in that region anchored at the crossing points. In many cases, the quadratic fit lies so close to it that it is indistinguishable from the fundamental + harmonic fit. In all 11 regions, the quadratic fit lies on the same side of the fundamental fit alone as the fundamental + harmonic fit. We therefore reject the hypothesis that the data are randomly distributed relative to the fundamental and, consequently, that the harmonic is not real, at the level of p-value $= 4.9 \times 10^{-4}$—i.e., 3.3σ.

Table 1
Cycles, Sections, and Regions of the Observations

Cycle	Section	Region	MJD Start	MJD End	Date Start	Date End
0	4	1	43619	45256	4/21/78	10/14/82
1	1	2	45256	46894	10/14/82	4/9/87
1	2	3	46894	48531	4/9/97	10/2/91
1	3	4	48531	50169	10/2/91	3/27/96
1	4	5	50169	51806	3/27/96	9/19/00
2	1	6	51806	53444	9/19/00	3/15/05
2	2	7	53444	55081	3/15/05	9/7/09
2	3	8	55081	56719	9/7/09	3/3/14
2	4	9	56719	58356	3/3/14	8/26/18
3	1	10	58356	59994	8/26/18	2/19/23
3	2	11	59994	61631	2/19/23	8/14/27

Note. The cycles are of duration equal to the period of the fundamental (6550 days). The sections are of duration of one half of the period of the harmonic—i.e., one-quarter of the period of the fundamental (1637.5 days). Thus, there are 11 separate regions of the light curve referred to in this Letter.

2. The harmonic, in addition to flattening out the minima in the light curve, creates higher peaks at the maxima.
3. In all 11 regions, throughout the whole light curve, the data alternate from side to side relative to the fundamental + trend fit (black curve) as time progresses. We have fitted quadratic polynomials, anchored to the fundamental + trend at the zero-points of the harmonic, to the data in each of the 11 regions. The parameters of these fits are given in Table 3 in Appendix B. The resulting fits are shown by the solid curves in the same color as the data in each region. As can be seen, these fits lie very close to the fundamental + trend + harmonic curve given by the green dashed line. The random probability of the data lying on the same side of the fundamental + trend as the harmonic in all 11 regions has p-value $= 4.9 \times 10^{-4}$, so this result is significant at the 3.3σ level.

Taken together, we find that these three points constitute compelling proof that the harmonic is real. This, in turn, proves that the fundamental is real and that these two periodicities in the light curve of PKS J1309+1154 are not a random result caused by the steep slope of the PSD. These three effects all result from the fact that the harmonic has a frequency twice that of the fundamental and is in phase with the fundamental.

3.1. The Folded Light Curve of PKS J1309+1154

In Figure 3(a), we show the folded light curve, based on the period of 6550 days, in which the light curves from Cycles 0, 2, and 3 have been folded onto that of Cycle 1 (see Table 1). In the folded curve, we delineate the four sections of the fundamental period by the vertical dashed lines, which mark the time when the harmonic amplitude is zero (where the green curve crosses the black curve). In Figure 3(a), the different cycles show clearly that the same pattern repeats in each cycle, with the main deviations from the fundamental+trend (black curve) repeating from one cycle to the next. The oscillation of the light curve from one side of the fundamental sine-wave fit to the other four times per period of the harmonic is very clear. In Figure 3(b), we have fitted quadratic polynomials (see the solid colored curves) anchored to the fundamental at the crossover points at the section boundaries, which illustrates this oscillating behavior very clearly. Note that the quadratic fits to the folded curve of Figure 3(b) are better in many cases than the quadratic fits of Figure 2, indicating that the coherence of the harmonic continues from one cycle to the next throughout the light curve.

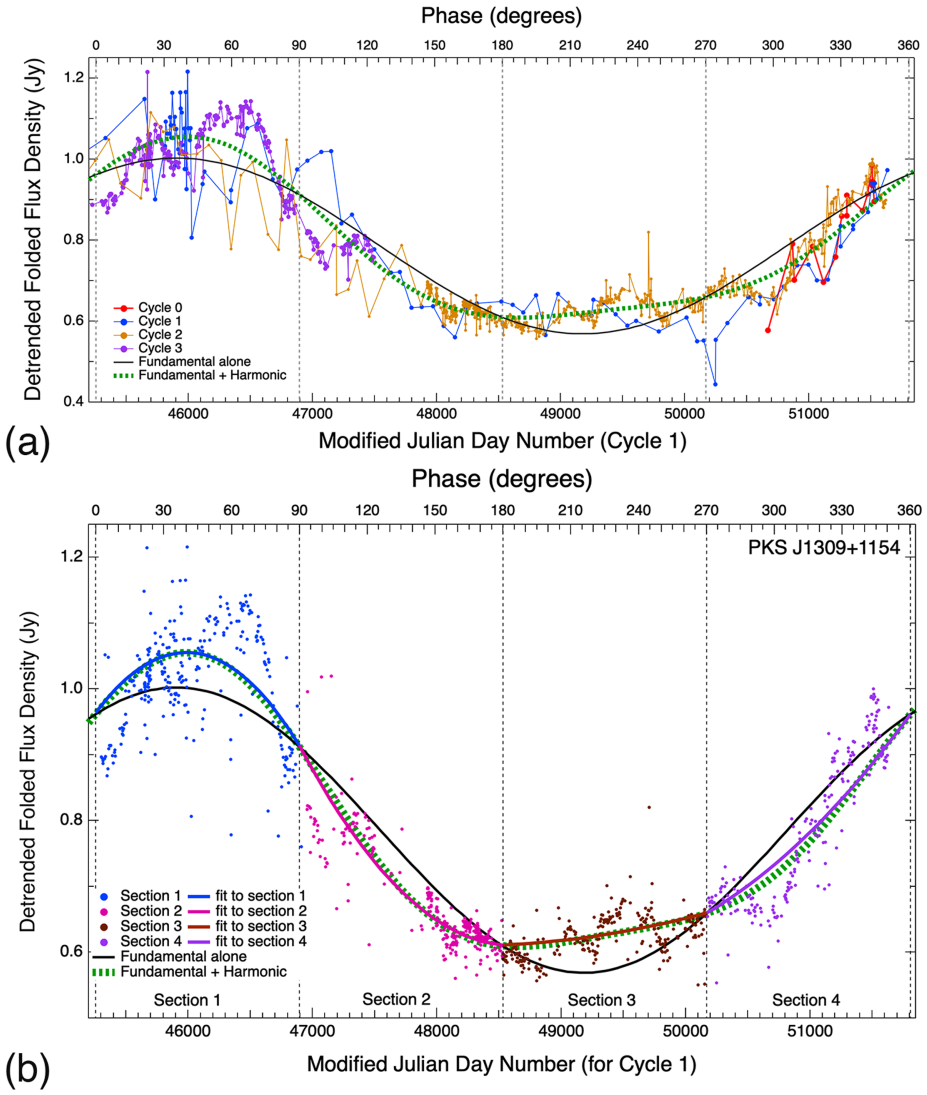

Figure 3. The detrended folded light curve of PKS J1309+1154, assuming a period of 6550 days for the fundamental periodicity. (a) The folded light curve showing the different cycles (see Table 1). Here, we have folded Cycles 0, 2, and 3 onto Cycle 1. (b) Here, the folded data have been divided into the four sections listed in Table 1. Least-squares fits of quadratic polynomials have been performed on each section separately, with the polynomials anchored at the zero-points of the harmonic, shown here by the crossover points of the fundamental versus the fundamental + harmonic fits. The resulting best fits are reported in Table 4. Rather surprisingly, these quadratic fits now lie almost identically on the fit of the fundamental + harmonic, showing clearly that the data are far more consistent with the fit including the harmonic than that excluding the harmonic. A comparison of the quadratic polynomial fits in Figure 2 with those in (b) above shows that some of these fits are significantly better in the folded light curve, indicating the coherence of the underlying fundamental + harmonic signal over the 2.57 cycle duration of the observations.

3.2. The Weighted Wavelet Z-transform Spectrum and the Duration of the Harmonic

We have also used the weighted wavelet *Z*-transform (WWZ; G. Foster 1996) to analyze the light curve of PKS J1309+1154. In Figures 4(a)–(d), we show WWZ spectra of the light curve of PKS J1309+1154. These make the presence of the harmonic clear. The four panels are as follows. (a) The fundamental, with a period of ∼17.9 yr, is clearly visible over the full 46 yr span of the observations. However, the harmonic is not visible in this figure. (b) Here, we have used the square root of the power, which enhances the harmonic relative to the fundamental. The harmonic is clearly visible up to 30 June, 2012. From 1 July, 2012, on, we have tested adding the OVRO data incrementally, 1 yr at a time, and again using the square root of the power. (c) Here, we see that the harmonic is clearly visible up to 2015. After 2015, the relative strength of the harmonic increases up to 2019. (d) This shows the harmonic strength increases with time compared to (c). Hereafter, the relative strength of the harmonic remains constant, but the width of the harmonic feature increases. These WWZ spectra demonstrate clearly that the harmonic feature is present and coherent over the whole 46 yr light curve. This is consistent with the fact that the quadratic fits shown in Figure 2 in Regions 10 and 11 continue to oscillate in phase with the harmonic. We interpret this as showing that the underlying harmonic is indeed present but is somewhat masked by the variations that are not related to the sinusoidal component. The critical test will be to see whether the light curve of PKS J1309 +1154 is approximately flat from 2026 to 2034.

4. Jetted SMBHB Interpretation

As in the cases of PKS 2131–021 and PKS J0805–0111 (Papers I–III; A. D. Hincks et al. 2025), one of the most natural explanations for a periodicity in PKS J1309+1154 is an

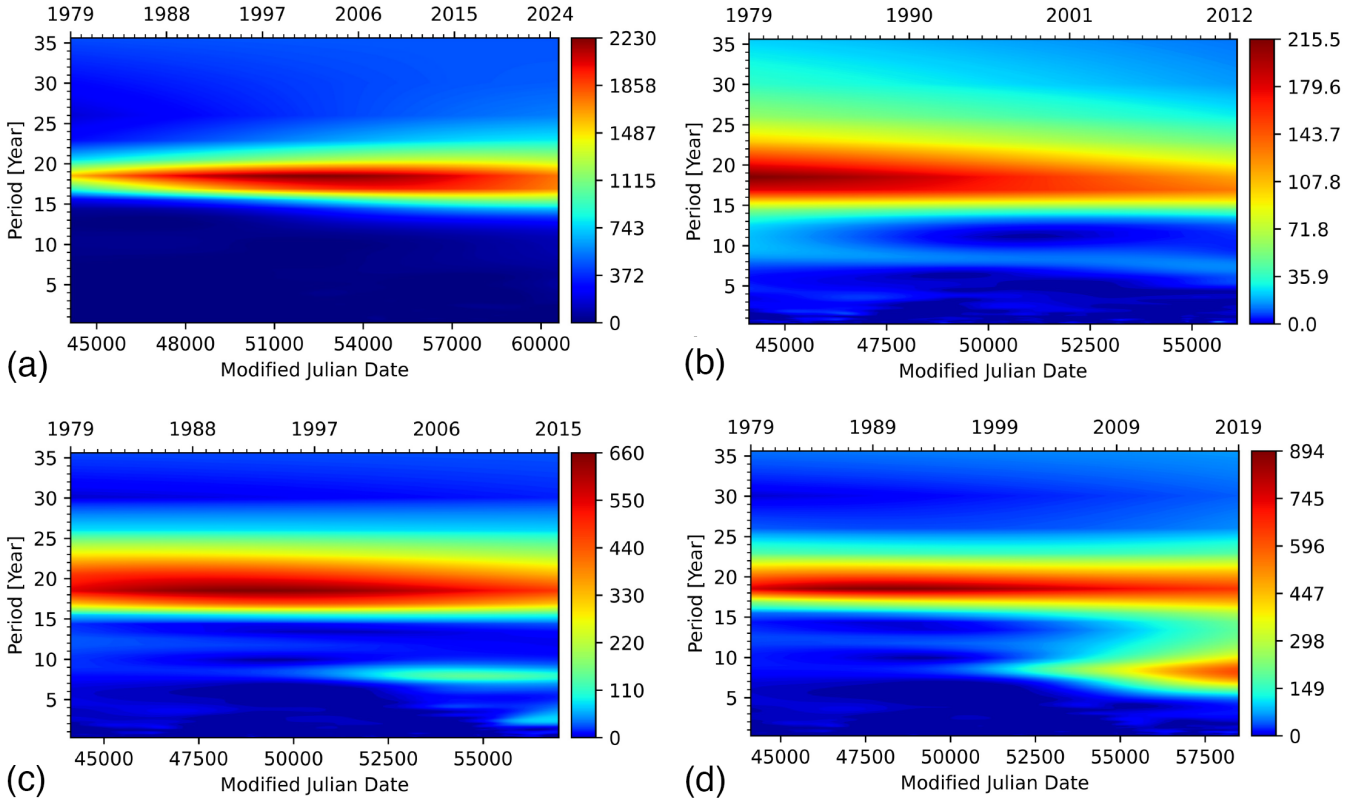

Figure 4. WWZ spectra of PKS J1309+1154 showing the fundamental periodicity and the first harmonic, which are both coherent over the whole light curve (see the text). (a) The spectrum of the full UMRAO+OVRO 46 yr light curve on the conventional linear power scale. (b)–(d) WWZ spectra using the square root of the power (see the text). (b) The spectrum of the full (1979– 30 June, 2012,) UMRAO light curve alone. The harmonic is clearly visible. (c) The spectrum of the full UMRAO light curve from 1979 to 30 June, 2012, plus the OVRO light curve from 1 July, 2012, to 2015. (d) The spectrum of the full UMRAO light curve from 1979 to 30 June, 2012, plus the OVRO light curve from 1 July, 2012 to 2019.

SMBHB with redshifted orbital period $P = 17.9$ yr. The jets, which produce the beamed radio emission seen in these systems, can be dragged by the binary orbital motion, leading to variable Doppler beaming (E. Sobacchi et al. 2017; Paper I). Paper IV proposed a model in which one black hole produces a jet, which is collimated by a subrelativistic disk wind. The orbital motion causes the wind to form a helical channel through which the relativistic jet flows (see the bottom panel of Figure 1 in Paper IV), and the redirection of the jet as it flows through the channel causes the change in beaming relative to the observer. The helix has a wavelength of $\lambda_h = \beta_w cP$, where β_w is the speed of the wind–jet boundary and consequently the pattern speed of the helix.

The jet is modeled as a synchrotron-emitting cone whose jet velocity direction is sinusoidally perturbed by an angle $\sim\beta_H/\beta_w$, where β_H is the orbital speed of the jet-launching black hole (Paper IV). We assume a power-law synchrotron spectrum from radius $r_{\rm min}$ to $r_{\rm max}$ and calculate the radiative transfer of the radio emission through the jet to determine the flux density. The model parameters are the electromagnetic power L_m, the power in radiating particles L_e, the bulk Lorentz factor of the jet Γ_j, the jet opening angle θ_j, β_w, β_H, the jet viewing inclination i, and the radiating electron/positron energy spectrum ranging from $\gamma_{e,\rm min}$ to $\gamma_{e,\rm max}$ with spectral index p. See Paper IV for more details.

While this model can explain the multiwavelength observations of PKS J0805–0111, PKS J1309+1154, and PKS 2131–021, it is important to note that it does not produce a clear first harmonic, so the harmonic in PKS J1309+1154 complicates the story. One possible explanation for the in-phase harmonic (or possible secondary maximum) is the emission from a weaker jet attached to the second black hole, which, in the model, amounts to adding the contribution of a second jet out of phase by $P/2$, assuming the orbit is circular. Additionally, to capture the effects of a harmonic, we cannot expand the variation in Doppler factor to lowest order in β_H. Instead, we must compute the full Doppler factor as a function of time.

Following Paper IV, we write the redirected radial unit vector of a particular position within the open jet $\hat{r}$ as

$$\hat{r}(t) = \frac{1}{\sqrt{1 + 2\hat{r}_0 \cdot \frac{\boldsymbol{\beta}_H}{\beta_w} + \frac{\beta_H^2}{\beta_w^2}}}\left(\hat{r}_0 + \frac{\boldsymbol{\beta}_H(t)}{\beta_w}\right), \quad (1)$$

where $\hat{r}_0$ is the unperturbed radial unit vector, which corresponds to a fixed direction in the black hole frame. $\boldsymbol{\beta}_H$ introduces sinusoidal perturbation to $\hat{r}$. At a particular radius r from the black hole, $\boldsymbol{\beta}_H$ in Equation (1) is delayed in phase from the instantaneous orbital velocity by r/λ_h. The local relativistic flow velocity in the observer frame is then $\boldsymbol{\beta}_j = \beta_j\hat{r}$, where β_j is the velocity associated with Γ_j. The jet Doppler factor is

$$D(t) = \frac{1}{\Gamma_j(1 - \beta_j(\hat{r}(t) \cdot \hat{n}))}, \quad (2)$$

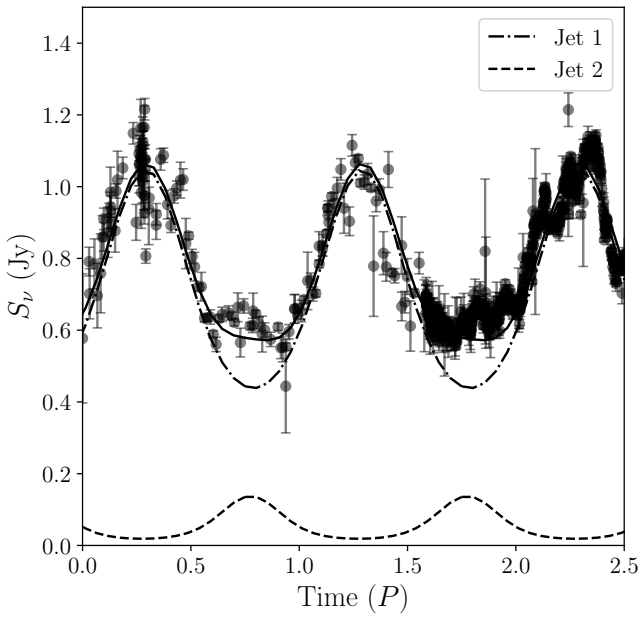

Figure 5. The proposed model for the detrended PKS J1309+1154 OVRO light curve using a modified version of the SMBHB jet model of Paper IV. Both black holes in the SMBHB have jets, but these are of unequal strength. The model jet parameters are listed in the text.

where $\hat{n}$ is the fixed observer direction. The flux density at the observed frequency ν for each jet is

$$S_\nu(t) = (1 + z_S)\, d_L^{-2} \iiint D(t)^{\frac{3+p}{2}} j'_{\nu_z,\Omega} e^{-\tau_\nu(t)} dV, \qquad (3)$$

where z_S is the source redshift, d_L is the luminosity distance, $\tau_\nu(t)$ is the optical depth (which depends on $D(t)$), and $j'_{\nu_z,\Omega}$ is the pitch-angle-averaged emissivity in the comoving frame given by the right-hand side of Equation (2) in Paper IV. For the volume element $dV = r^2 \sin\chi dr d\chi d\psi$, the integration bounds are $r \in [r_{\rm min}, r_{\rm max}]$, $\chi \in [0, \theta_j]$, and $\psi \in [0, 2\pi]$. The main difference between this treatment and that presented in Paper IV is that here we treat the variation in D and consequently S_ν nonperturbatively. We evaluate Equation (3) for two jets and sum them to get the total emission.

In Figure 5, we show a plausible model light curve for PKS J1309+1154, including the contributions of each of the two jets. Since there is no reliable redshift for this source, we assume $z_S = 1.3$, similar to PKS 2131–021 and PKS J0805–0111. We choose a nominal $i = 4°$ inclination. For the primary jet, we take $L_{e,1} = 7 \times 10^{45}\,{\rm erg\,s^{-1}}\,(r/r_0)/(1 + (r/r_0))$ (where $r_0 = 5$ ly), $L_{m,1} = 7 \times 10^{45}\,{\rm erg\,s^{-1}}\,1/(1 + (r/r_0))$, $\theta_{j,1} = 0.05$, and $\Gamma_{j,1} = 15$. The scaling is chosen so that $L_{j,1} = L_{m,1} + L_{e,1}$ remains constant. We assume the particle spectrum is initialized with $\gamma_{e,\rm min} = 10$, $\gamma_{e,\rm max} = 300$, and $p = 1.2$ across the jet, with normalization set by $L_{e,1}(r)$. The flatness in the spectrum makes it difficult to know the precise spectral index. These choices would be consistent with magnetic reconnection as the dominant electron/positron acceleration mechanism, although the acceleration mechanism remains unknown in these sources (Paper IV). We choose $\beta_{w,1} = 0.9$, $\beta_{H,1} = 0.02$, $r_{\rm min}$ so that $\tau_\nu(r_{\rm min}) = 20$, and $r_{\rm max} = r_{\rm min} + 100$ ly $(\nu(1+z)/15\,{\rm GHz})^{-1}$. For the secondary jet, we keep all parameters the same, except we take $L_{e,2} = 1 \times 10^{45}\,{\rm erg\ s^{-1}}\,(r/r_0)/(1 + (r/r_0))$, $L_{m,2} = 1 \times 10^{45}\,{\rm erg\ s^{-1}}\,1/(1 + (r/r_0))$, and $\beta_{H,2} = 0.4$ corresponding to a mass ratio of $q = 0.5$. These parameters—particularly L_j, Γ_j, θ_j, and $r_{\rm max}$—differ from those used in PKS 2131–021 and PKS J0805–0111 (Paper IV). The changes made accommodate the sharper peaks seen in the 2.5 cycles of the primary jet.

The main parameter governing the relative heights of the peaks is the relative values of L_j between the two jets. Since we are only modeling the light curve at one observing frequency (15 GHz), and the wind speed cannot be well constrained in our model, the quoted parameters are meant to be illustrative and can be more confidently constrained with multiwavelength light curves and a more precise redshift.

As a consistency check, we can also estimate the corresponding mass ratio of the binary, assuming for simplicity that the difference in luminosity was solely a result of different accretion rates onto the two black holes at orbital scales. Under those assumptions, and using a fit of the mass-accretion-rate ratios from hydrodynamical simulations (D. Lai & D. J. Muñoz 2023), we then estimate a binary mass ratio $q \simeq 0.5$.

There are various issues with explaining the possible secondary maximum with a dual jet. If the opening angle $\theta_j > \beta_H/\beta_w$ for both jets or if $\beta_{w,1} \neq \beta_{w,2}$, the jets will crash into one another and likely merge into one jet. If this is the case, it is unlikely that there would be two stable jets to produce clean light-curve peaks. There are other models in which one jet can produce the variation, due to the internal structure of the jet.

If there is a secondary maximum in the light curve of a source like J1309, then it is possible to account for it in the context of a single jet, in principle at least, by invoking a more complicated model of the emissivity than we have used so far. If we suppose that the jet rest-frame emissivity is uniform on spherical surfaces within the jet, then it is easy to see that the observed flux will exhibit one maximum and one minimum within an orbital period. The flux, though, need not be sinusoidal. The first complication is to allow the jet Lorentz factor to vary with polar angle χ within the jet. A variation $\Gamma_j \propto (r \sin\chi)^{-1}$ can comply with the causality constraint and accommodate the presence of a sheath. Allowing L_j to vary with χ can also lead to an edge-brightened jet. The second complication arises from the variation of the emissivity with the jet azimuth ψ. In the model, the jet is confined and directed by the surrounding wind. Due to the orbital motion, individual jet elements are flowing into the wind asymmetrically, which could lead to the leading side possessing a higher emissivity than the trailing side (i.e., higher L_j on the side of the jet moving into the wind). A model including these features may be able to produce the observed secondary maximum. A more complicated formalism, capable of exhibiting these effects, will be presented elsewhere.

We caution that, in principle, other potential explanations for the harmonics in these sources have been proposed besides SMBHB motion, including accretion-disk modes (T. An et al. 2013) and (first) harmonics associated with disk tearing and precession (G. Musoke et al. 2023). It is also possible that some global jet mode may produce this emission. All of these alternative explanations raise potential questions about long-term period and harmonic stability. Of course, with only 2.57 cycles of the fundamental observed thus far, continued monitoring will be needed to determine the stability.

5. Discussion

It is important to recognize that the emission from blazars at radio wavelengths is well known to originate in multiple regions along the jet (see, e.g., Papers I and and IV). Therefore, not all of the emission in PKS J1309+1154 comes from the zone that is responsible for the sinusoidal variations. In particular, (i) the regions giving rise to the long-term trend are not those producing the sinusoidal variations, and (ii) the short-term deviations from the sinusoidal emission originate in emission regions that are not related to the sinusoidal emission, as discussed in detail in Paper I.

The combined UMRAO+OVRO light curve of PKS J1309 +1154 and the detailed analysis in Section 3 amount, in our view, to a compelling argument that the periodicities related to the fundamental and harmonic are caused by an underlying periodicity in the blazar itself, most likely in its central engine, and are not a random product of the steep slope of the PSD. We regard this evidence as conclusive for the following two reasons:

1. The least-squares quadratic fits to the data in the 11 regions separated by the zero-points in the first harmonic clearly lie on the same side of the fundamental curve as the fundamental + harmonic curve. In other words, the data switch sides coherently with the harmonic in all 11 regions. On the null hypothesis that the harmonic is not real, the data should be randomly distributed on either side of the fundamental curve, so the probability of this happening by chance has a p-value $= 4.9 \times 10^{-4}$—i.e., this result is significant at the 3.3σ level.
2. The light curve displays two comparatively flat 8 yr long sections, from 1990 to 1998 and again from 2008 to 2016. The fundamental + harmonic curve likewise displays flat regions over these two 8 yr windows, whereas the fundamental curve alone does not.

For these reasons, we find the evidence for the harmonic compelling. This, of course, makes the evidence for the fundamental equally strong. This is the first time, to our knowledge, that such clear evidence for a fundamental periodicity and a harmonic periodicity has been found in a blazar light curve.

These results for PKS J1309+1154 provide conclusive evidence that some blazar light curves exhibit real physical sinusoidal periodicities that are very likely produced in the central engine. We regard the light curve of PKS J1309+1154 as providing the strongest evidence yet that some of the sinusoidal variations appearing in blazar light curves are real and not a result of the steep slope of the PSD. The fact that we now know that some sinusoidal variations are real greatly strengthens the case for the same interpretation of the light curves of PKS J0805–0111 (P. V. de la Parra et al. 2025) and, in particular, of PKS 2131–021 (Papers I and II), given that these both easily passed our 3σ test based on simulations. Furthermore, the fact that in PKS 2131–021 coherent sinusoidal variations are seen at optical wavelengths shows that this sinusoidal emission persists all the way back, from the radio-emitting regions, to a region very close to the central engine itself, where the emission must be very nearly in phase with the physical mechanism in the central engine that is producing the periodicity, thus revealing the phase, as well as the period, of this mechanism.

The discovery of a compelling first harmonic in a blazar light curve opens up a new dimension to searches for SMBHB candidates, because it provides, for the first time, a strong *predictive* test of any periodicities that might be found. While not all SMBHB candidates will necessarily have first harmonics, the fact that one has been found among the first three sinusoidally varying strong SMBHB candidates (PKS J0805–0111, PKS J1309+1154, and PKS 2131–021) to be found in radio light curves suggests that a significant fraction of SMBHB candidates found in radio blazar light curves are likely to have detectable first harmonics.

We estimate (Paper II) that ~1 in 100 blazars is an SMBHB candidate. Thus, given that the South Pole Telescope (95 GHz, 150 GHz, and 220 GHz; J. E. Carlstrom et al. 2011; B. A. Benson et al. 2014), the Simons Observatory (27 GHz–285 GHz; P. Ade et al. 2019; M. Abitbol et al. 2025), and the Vera Rubin Observatory (320–1060 nm; B. Czerny et al. 2023) will be monitoring tens of thousands of blazars over at least a 10 yr period, we estimate that, applying the filter of a first harmonic search for identifying SMBHB candidates and hence proving the periodicity is real, they will identify tens, if not hundreds, of such candidates for which the redshift, the period, and the phase of the periodicities will be known. This will enable powerful searches for gravitational waves from these objects. The remaining unknowns are the orbital velocities of the SMBHBs. This will motivate intensive searches for optical and infrared spectral-line variations due to orbital motion, which, if identified, would yield the masses of the two binary components.

This information would then make possible a fully coherent "matched-filter" search for gravitational waves from a network of SMBHBs for which the periods, phases, and amplitudes of the expected gravitational waves from each individual SMBHB candidate would be known. Since the directions, amplitudes, and phases of all these individual gravitational-wave signals would be known, they could all be summed *with the correct relative phases, and hence coherently,* and with the correct amplitudes, making possible a fully coherent search for gravitational waves from the network of SMBHB candidates.

For the above reasons, we believe that the discovery of compelling evidence for a first harmonic in the combined UMRAO+OVRO light curve of the blazar PKS J1309+1154 is a major breakthrough in the quest for periodicities in blazars that are likely due to SMBHBs, making them promising targets for searches for gravitational waves using pulsar timing arrays.

Acknowledgments

This work is supported by NSF grants AST2407603 and AST2407604. We thank the California Institute of Technology and the Max Planck Institute for Radio Astronomy for supporting the OVRO 40 m program. Without this private support, this program would have ended in 2016. We also thank all the volunteers who have enabled this work to be carried out. Prior to 2016, the OVRO program was supported by NASA grants NNG06GG1G, NNX08AW31G, NNX11A043G, and NNX13AQ89G, from 2006 to 2016, and NSF grants AST-0808050 and AST-1109911, from 2008 to 2014. The UMRAO program received support from NSF grants AST-8021250, AST-8301234, AST-8501093, AST-8815678, AST-9120224, AST-9421979, AST-9900723, AST-0307629, AST-0607523, and earlier NSF awards, and from NASA grants NNX09AU16G, NNX10AP16G, NNX11AO13G,

and NNX13AP18G. Additional funding for the operation of UMRAO was provided by the University of Michigan. W.M. acknowledges support from ANID project Basal FB210003. A.S. and R.B acknowledge support from a grant from the Simons Foundation (00001470, RB, AS). Y.D. and F.A.H. acknowledge support through NASA under contract No. NNG08FD60C. R.R. and B.M. and P.V.d.l.P. acknowledge support from ANID Basal AFB-170002, Núcleo Milenio TITANs (NCN2023_002), CATA BASAL FB210003, and UdeC-VRID 2025001479INV. T.H. acknowledges support from the Academy of Finland projects 317383, 320085, 345899, and 362571 and from the European Union ERC-2024-COG—PARTICLES—101169986. K.T. acknowledges the support from the TITAN ERA Chair project (contract no. 101086741) within the Horizon Europe Framework Program of the European Commission. This research is partially funded by the European Union. The views and opinions expressed are, however, those of the author(s) only and do not necessarily reflect those of the European Union or the European Research Council Executive Agency. Neither the European Union nor the granting authority can be held responsible for them. V.P. is supported by an ERC grant, mw-atlas project No. 101166905. I.L is funded by the European Union ERC-2022-STG—BOOTES—101076343.

Facilities: OVRO:40 m, UMRAO, NRAO: VLBA, ALMA, WISE.

Appendix A
Sine-wave Fitting

We fitted a model that includes two sine waves with periods P and $P/2$ and a linear trend to the light curve of PKS J1309+1154. In this model, the flux density is given by

$$S(t) = S_0 + A_1 \sin(\phi(t) - \phi_{0,1}) + A_2 \sin(2\phi(t) - \phi_{0,2}) + \beta(t - t_0)/365.25, \quad \text{(A1)}$$

where $\phi(t) = 2\pi(t - t_0)/P$ and $t_0 = 52{,}000$. Here, P is the fundamental period, A_1 and A_2 are amplitudes of the fundamental and the harmonic, $\phi_{0,1}$ and $\phi_{0,2}$ are their phases at $t = t_0$, and S_0 is the mean flux density. We found the best-fit parameters by maximizing the following likelihood function:

$$\ln \mathcal{L} = -\frac{1}{2}\sum_i \left[\frac{(S_i - S(t_i))^2}{\sigma_i^2 + \sigma_0^2} + \ln(\sigma_i^2 + \sigma_0^2) \right], \quad \text{(A2)}$$

where σ_0 is a parameter that accounts for additional scatter in the data that is not captured by the original error bars. We used the Markov Chain Monte Carlo sampler by D. Foreman-Mackey et al. (2013) to derive the posterior distributions for all model parameters. The resulting best-fit values are reported in Table 2.

Table 2
Best-fit Parameters of the Sine-wave Model for PKS J1309+1154

Parameter	Value
P (days)	6550 ± 19
A_1 (Jy)	0.2167 ± 0.0022
A_2 (Jy)	0.0543 ± 0.0022
$\phi_{0,1}$ (rad)	−1.133 ± 0.017
$\phi_{0,2}$ (rad)	−0.372 ± 0.055
β (Jy yr^{-1})	−0.00769 ± 0.00018
S_0 (Jy)	0.7856 ± 0.0027
σ_0 (Jy)	0.0440 ± 0.0012

Appendix B
Quadratic Fits

We then fitted a quadratic polynomial to each region of the light curve, as defined in Table 1. We anchored the polynomial at the crossing points of the fundamental and the harmonic. Assuming that the polynomial crosses points (x_1, S_1) and (x_2, S_2), the flux density can be expressed as follows:

$$S(x) = S_1 + \frac{S_2 - S_1}{x_2 - x_1}(x - x_1) + p(x - x_1)(x - x_2), \quad \text{(B1)}$$

where p is a parameter and $x \equiv (t - t_1)/365.25$. The best-fit value of p and its uncertainty were calculated by maximizing the likelihood function defined in Equation (A2). The resulting best fits for the eleven regions in Figure 2 are reported in Table 3, and the resulting best fits for the four sections in Figure 3(b) are reported in Table 4.

Table 3
Best-fit Parameters of the Quadratic Polynomial Fits for PKS J1309+1154

Region	t_1	t_2	S_1	S_2	p	σ_0
1	43,619	45,256	0.8355	1.1035	0.0000 ± 0.0040	0.0223 ± 0.0159
2	45,256	46,894	1.1035	1.0196	−0.0222 ± 0.0032	0.0812 ± 0.0119
3	46,894	48,531	1.0196	0.6828	0.0103 ± 0.0050	0.0735 ± 0.0183
4	48,531	50,169	0.6828	0.6976	0.0039 ± 0.0033	0.0422 ± 0.0134
5	50,169	51,806	0.6976	0.9655	0.0161 ± 0.0031	0.0494 ± 0.0097
6	51,806	53,444	0.9655	0.8817	−0.0156 ± 0.0056	0.0749 ± 0.0229
7	53,444	55,081	0.8817	0.5448	0.0123 ± 0.0006	0.0191 ± 0.0017
8	55,081	56,719	0.5448	0.5597	0.0009 ± 0.0005	0.0197 ± 0.0014
9	56,719	58,356	0.5597	0.8276	0.0047 ± 0.0010	0.0466 ± 0.0028
10	58,356	59,994	0.8276	0.7438	−0.0248 ± 0.0011	0.0593 ± 0.0032
11	59,994	61,631	0.7438	0.4069	0.0152 ± 0.0024	0.0550 ± 0.0064

Table 4
Best-fit Parameters of the Quadratic Polynomial Fits for PKS J1309+1154

Section	t_1	t_2	S_1	S_2	p	σ_0
1	45,256	46,894	0.9641	0.9141	−0.0229 ± 0.0011	0.0633 ± 0.0029
2	46,894	48,531	0.9141	0.6111	0.0138 ± 0.0007	0.0330 ± 0.0018
3	48,531	50,169	0.6111	0.6598	0.0017 ± 0.0005	0.0211 ± 0.0013
4	50,169	51,806	0.6598	0.9615	0.0061 ± 0.0010	0.0482 ± 0.0026

ORCID iDs

A. C. S. Readhead https://orcid.org/0000-0001-9152-961X
M. F. Aller https://orcid.org/0000-0003-2483-2103
A. G. Sullivan https://orcid.org/0000-0002-9545-7286
R. D. Blandford https://orcid.org/0000-0002-1854-5506
P. Mróz https://orcid.org/0000-0001-7016-1692
P. V. De la Parra https://orcid.org/0000-0001-5957-1412
B. Molina https://orcid.org/0009-0000-9963-6874
E.R. Most https://orcid.org/0000-0002-0491-1210
M. L. Lister https://orcid.org/0000-0003-1315-3412
A. Synani https://orcid.org/0009-0004-2614-830X
H. Aller https://orcid.org/0000-0003-1945-1840
M. C. Begelman https://orcid.org/0000-0003-0936-8488
Y. Ding https://orcid.org/0000-0002-5770-2666
M. J. Graham https://orcid.org/0000-0002-3168-0139
F. Harrison https://orcid.org/0000-0002-4226-8959
T. Hovatta https://orcid.org/0000-0002-2024-8199
I. Liodakis https://orcid.org/0000-0001-9200-4006
W. Max-Moerbeck https://orcid.org/0000-0002-5491-5244
V. Pavlidou https://orcid.org/0000-0002-0870-1368
T. J. Pearson https://orcid.org/0000-0001-5213-6231
V. Ravi https://orcid.org/0000-0002-7252-5485
R. A. Reeves https://orcid.org/0000-0001-5704-271X
T. Surti https://orcid.org/0000-0002-6369-6266
K. Tassis https://orcid.org/0000-0002-8831-2038
S. E. Tremblay https://orcid.org/0000-0001-7662-2576
J. A. Zensus https://orcid.org/0000-0001-7470-3321

References

Abitbol, M., Abril-Cabezas, I., Adachi, S., et al. 2025, JCAP, 2025, 034
Ade, P., Aguirre, J., Ahmed, Z., et al. 2019, JCAP, 2019, 056
Agarwal, N., Agazie, G., Anumarlapudi, A., et al. 2025, arXiv:2508.16534
Agazie, G., Anumarlapudi, A., Archibald, A. M., et al. 2023a, ApJL, 951, L8
Agazie, G., Anumarlapudi, A., Archibald, A. M., et al. 2023b, ApJL, 952, L37
Agazie, G., Anumarlapudi, A., Archibald, A. M., et al. 2023c, ApJL, 951, L50
Aller, H. D., Aller, M. F., Latimer, G. E., & Hodge, P. E. 1985, ApJS, 59, 513
Aller, M. F., Hughes, P. A., Aller, H. D., Latimer, G. E., & Hovatta, T. 2014, ApJ, 791, 53
An, T., Baan, W. A., Wang, J.-Y., Wang, Y., & Hong, X.-Y. 2013, MNRAS, 434, 3487
Backer, D. C., Kulkarni, S. R., Heiles, C., Davis, M. M., & Goss, W. M. 1982, Natur, 300, 615
Begelman, M. C., Blandford, R. D., & Rees, M. J. 1980, Natur, 287, 307
Begelman, M. C., Blandford, R. D., & Rees, M. J. 1984, RvMP, 56, 255
Benson, B. A., Ade, P. A. R., Ahmed, Z., et al. 2014, SPIE, 9153, 91531P
Blandford, R., Meier, D., & Readhead, A. 2019, ARA&A, 57, 467
Britzen, S., Fendt, C., Witzel, G., et al. 2018, MNRAS, 478, 3199
Carlstrom, J. E., Ade, P. A. R., Aird, K. A., et al. 2011, PASP, 123, 568
Ciaramella, A., Bongardo, C., Aller, H. D., et al. 2004, A&A, 419, 485
Czerny, B., Panda, S., Prince, R., et al. 2023, A&A, 675, A163
de la Parra, P. V., Kiehlmann, S., Mróz, P., et al. 2025, ApJ, 987, 191
EPTA Collaboration, InPTA Collaboration, Antoniadis, J., et al. 2023, A&A, 678, A50
Foreman-Mackey, D., Hogg, D. W., Lang, D., & Goodman, J. 2013, PASP, 125, 306
Foster, G. 1996, AJ, 112, 1709
Hincks, A. D., Ma, X., Naess, S. K., et al. 2025, arXiv:2504.04278
Hodgson, J. A., Krichbaum, T. P., Marscher, A. P., et al. 2017, A&A, 597, A80
Hughes, P. A., Aller, H. D., & Aller, M. F. 1998, ApJ, 503, 662
Kiehlmann, S., de la Parra, P. V., Sullivan, A. G., et al. 2025, ApJ, 985, 59
Komatsu, E., Dunkley, J., Nolta, M. R., et al. 2009, ApJS, 180, 330
Komossa, S., Grupe, D., & Kraus, A. 2023, MNRAS, 522, L84
Lai, D., & Muñoz, D. J. 2023, ARA&A, 61, 517
Lehto, H. J., & Valtonen, M. J. 1996, ApJ, 460, 207
Lomb, N. R. 1976, Ap&SS, 39, 447
Miles, M. T., Shannon, R. M., Reardon, D. J., et al. 2025, MNRAS, 536, 1489
Molina, B., Mróz, P., De la Parra, P. V., et al. 2025, arXiv:2510.23103
Musoke, G., Liska, M., Porth, O., van der Klis, M., & Ingram, A. 2023, MNRAS, 518, 1656
O'Neill, S., Kiehlmann, S., Readhead, A. C. S., et al. 2022, ApJL, 926, L35
Pihajoki, P., Valtonen, M., & Ciprini, S. 2013, MNRAS, 434, 3122
Planck Collaboration, Aghanim, N., Akrami, Y., et al. 2020, A&A, 641, A6
Readhead, A. C. S. 2024, JAHH, 27, 453
Readhead, A. C. S., & Hewish, A. 1974, MmRAS, 78, 1
Readhead, A. C. S., Lawrence, C. R., Myers, S. T., et al. 1989, ApJ, 346, 566
Richards, J. L., Max-Moerbeck, W., Pavlidou, V., et al. 2011, ApJS, 194, 29
Scargle, J. D. 1982, ApJ, 263, 835
Sobacchi, E., Sormani, M. C., & Stamerra, A. 2017, MNRAS, 465, 161
Sullivan, A. G., Blandford, R. D., Synani, A., et al. 2025, arXiv:2510.02301
Valtonen, M. J. 2007, ApJ, 659, 1074
Valtonen, M. J., Lehto, H. J., Nilsson, K., et al. 2008, Natur, 452, 851
Valtonen, M. J., Zola, S., Ciprini, S., et al. 2016, ApJL, 819, L37
Valtonen, M. J., Zola, S., Gopakumar, A., et al. 2023, MNRAS, 521, 6143
Zechmeister, M., & Kürster, M. 2009, A&A, 496, 577
Zic, A., Reardon, D. J., Kapur, A., et al. 2023, PASA, 40, e049